# Adopting the $I_3$–$R_{24}$ rainfall index and landslide susceptibility for the establishment of an early warning model for rainfall-induced shallow landslides

Lun-Wei Wei[1,3], Chuen-Ming Huang[2,3], Hongey Chen[1,4], Chyi-Tyi Lee[2], Chun-Chi Chi[5], and Chen-Lung Chiu[5]

[1]Department of Geosciences, National Taiwan University, Taiwan

[2]Institute of Applied Geology, National Central University, Taiwan

[3]Disaster Disaster Prevention Technology Research Center, Sinotech Engineering Consultants, INC., Taiwan

[4]National Science and Technology Center for Disaster Reduction, Taipei, Taiwan

[5]Central Geological Survey, MOEA, Taiwan

*Correspondence to*: Lun-Wei Wei (d03224007@ntu.edu.tw)

**Abstract.** Rainfall-induced landslides number among the most devastating natural hazards in the world, and early warning models are urgently needed to reduce losses and fatalities. Most landslide early warning systems are based on rainfall thresholds defined on the regional scale, regardless of the different landslide susceptibilities of various slopes. Here we divided slope units in southern Taiwan into three categories (high, moderate, and low) according to their susceptibility. For each category, we established separate rainfall thresholds so as to provide differentiated thresholds for different degrees of susceptibility. Logistic regression (LR) analysis was performed to evaluate landslide susceptibility by using event-based landslide inventories and predisposing factors. Analysis of rainfall patterns of 941 landslide cases gathered from field investigation led to the recognition that 3-hour mean rainfall intensity ($I_3$) is a key rainfall index for rainfall of short duration but high intensity; on the other hand, 24-hour accumulated rainfall ($R_{24}$) was recognized as a key rainfall index for rainfall of long duration but low intensity. Thus, the $I_3$–$R_{24}$ rainfall index was used to establish rainfall thresholds in this study. Finally, an early warning model is proposed by setting alert levels including yellow (advisory), orange (watch) and red (warning) according to a hazard matrix. These differentiated thresholds and alert levels can provide essential information for local governments to use in deciding whether to evacuate residents.

**Keywords:** rainfall-induced landslide, landslide susceptibility analysis, rainfall threshold, early warning

## 1 Introduction

Rainfall-induced landslides number among the most perilous natural hazards, causing severe casualties and economic losses worldwide (Ayalew, 1999; Evans et al., 2007; Tsou et al., 2011; Petley, 2012; Wang et al., 2015; Iverson et al., 2015; Sassa et al., 2015; Fan et al., 2017). Therefore, many efforts have been made to evaluate landslide susceptibility and thereby set criteria for issuing alerts that can save lives and property.

Landslides can be triggered by either rainfall or earthquakes (Dadson et al., 2003; Lee et al., 2004; Lin et al., 2008; Chen et al., 2011). In Taiwan, monsoons and typhoons bring great amounts of rainfall, up to 3,000 mm/year, and numerous landslides cause casualties every year. Therefore, recognizing the areas where rainfall-induced landslides might occur is an urgent issue. Here we adopted statistical method for the analysis of landslide susceptibility based on the assumption that the predisposing factors that cause landslides in a region are similar and can be used for predicting the locations of landslides in the future

(Guzzetti et al., 1999). In previous researches, several statistical models have been proposed as well as widely utilized in landslide susceptibility analysis, and logistic regression were one of the most used methods (Guzzetti et al., 1999; Lee et al., 2004, 2008a, 2008b, 2014).

On the other hand, rainfall thresholds for landslides can be categorized as either statistical approaches or deterministic approaches. In the former method, thresholds are decided by collecting historical landslide cases and analyzing their rainfall parameters and the probability lines of rainfall conditions (Caine, 1980; Guzzetti et al., 2008). In the latter method, thresholds are decided by calculating the safety factors of each slope or grid with geomaterial and rainfall parameters (Terlien, 1998; Kim et al., 2010). Statistical rainfall thresholds for shallow landslides have been well discussed (Guzzetti et al., 2007). They can be classified mainly into 5 categories: intensity-duration (Brunetti et al., 2010; Zhou et al., 2014; Pradhan et al., 2017), accumulated rainfall-duration (Martelloni, 2011; Rosi et al., 2012; Vessia et al., 2014; Gariano et al., 2015; Rossi et al., 2017), accumulated rainfall (Corominas and Moya, 1999; Bell and Maud, 2000), intensity-accumulated rainfall (Hong et al., 2005), and accumulated rainfall-accumulated rainfall (Osanai et al., 2010; Turkington et al., 2014).

Most of the studies set only one threshold for their study areas despite differences in the physical settings (geology, geomorphology, and meteorological conditions) of the regions. Recently, some studies have subdivided their study areas into several homogeneous sub-zones to discuss the influence of physical settings on thresholds (Hong and Adler, 2008; Segoni et al., 2014, 2015; Lee et al., 2015; Rosi et al., 2015, 2016; Peruccacci et al., 2017). However, for a smaller area such as slope units, differences in susceptibility may lead to different warning thresholds (Yang and Adler, 2008; Segoni et al., 2015; Lee et al., 2015). For example, the warning threshold of a high-susceptibility slope is likely to be lower than that of a low-susceptibility slope. To reduce this gap in knowledge, we focused on shallow landslides of the debris fall, debris topple, debris slide, earth fall, earth topple, and earth slide types proposed by Varnes (1978) and divided slope units according to three different landslide susceptibility levels (high, moderate, and low). After that, we established their rainfall thresholds separately. Furthermore, we set alert levels by adopting a hazard matrix and examined whether differentiated warning thresholds for different degrees of susceptibility existed. Moreover, given the importance of validating the performance of a landslide early warning model, especially the false alarms and missed alarms, to make it feasible for further practical application (Calvello et al. 2015; Devoli et al. 2015; Piciullo et al. 2017; Segoni et al., 2018), we also adopted skill scores to verify our results.

## 2 Study area

Taiwan is located in the western Pacific Ocean, on the convergent plate boundary zone of the Philippine Sea plate and the Eurasian plate. The orogenic uplift rate is 5–7 mm/year (Willett et al., 2003); however, the exhumation rate is also as high as 3–6 mm/year (Dadson et al., 2003) due to the fractured geological materials and the high mean annual precipitation of 2,500–3,000 mm brought by typhoons and monsoons every year (Hsu, 2013). The frequent natural disasters and high population density (23 million people in 36,000 km$^2$) of Taiwan make it one of the countries most exposed to multiple hazards (Dilley et al., 2005).

The study area, located in southern Taiwan (red box in Fig. 1), includes a mosaic of 47 1:25,000 scale maps (about 7,258.5 km$^2$) and covers densely inhabited and landslide-threatening hillslopes. The elevation ranges from 3,243 meters in mountain areas to 0 meters in plain areas, while the gradient ranges from 87º to 0º. The lithological units are mainly sedimentary rocks composed of sandstone, shale, mudstone, and conglomerate in the Western Foothills, as well as metamorphic rocks composed of slate, argillite and metasandstone in the Central Range.

## 3 Available data

### 3.1 Landslide inventory

Landslide inventories are essential for the assessment of landslide susceptibility or spatio-temporal land changes (Van Westen et al., 2003; Guzzetti et al., 2012; Samia et al., 2017; Valenzuela et al., 2017). Four procedures for the generation of rainfall-induced landslide inventories were followed in this study. First, barren lands were interpreted manually from SPOT 5 images by drawing polygons in ESRI ArcGIS software. Second, aerial photographs and satellite images from Google Earth software were applied to identify whether the barren lands were landslides or agricultural land. In addition, the polygons situated on slopes having gradients greater than 55 degrees were marked as rockfalls according to the classification rules proposed by the Central Geological Survey, Taiwan (Central Geological Survey, 2008). Polygons marked as agricultural land or rockfalls were deleted from the inventories to ensure that only shallow landslides would be analyzed in the study. Third, we randomly selected landslides from inventories and verified the correctness of the locations and boundaries by fieldwork. Finally, event-based landslide inventories, including newly-generated landslides and expanded landslides, were identified by comparing inventories before and after each event. In the end, 6 heavy rainfall events that triggered landslides were chosen, and a total of seven landslide inventories were generated in this study (Table 1).

### 3.2 Landslide occurrence time and field investigation

Rainfall conditions such as intensity, duration, and accumulated rainfall that induced landslides are key data in application of statistical methods to establish the rainfall thresholds for landslides (Guzzetti et al., 2007, 2008; Brunetti et al., 2010; Peruccacci et al., 2017). To analyze the rainfall conditions for each landslide case used in this study, a flowchart was proposed (Fig. 2). During field investigations, we verified the correctness of the landslide inventories and interviewed local residents to try to acquire the landslide occurrence times, since this information is rarely included in landslide inventories. The accuracy of landslide occurrence times is hard to evaluate due to the lack of video records; however, we focused on interviewing as many residents whose relatives were injured or houses were damaged/destroyed by the landslides as possible. Given the deep impressions left by such memories, we believe that the quality of landslide occurrence times might be improved. On the other hand, detailed characteristics of the landslides, such as lithology, geological structure, joint, strength, area, depth and mechanism, were also recorded during the field work. Finally, 941 landslide cases, including their occurrence times (date and hour) and the characteristics of the landslides, were gathered for further analysis.

### 3.3 Slope units

Slope units were used for the analysis of landslide susceptibility in this study (Carrara, 1988; Carrara et al., 1991, 1995; Guzzetti et al., 1999; Schlögel et al., 2017; Yang, 2017). To delineate the boundaries of slope units, 5×5m digital elevation models (5m DEMs) were acquired from the Ministry of the Interior, Taiwan. However, to reduce noise, we developed a Fortran program to obtain smoothed and resolution-reduced 10×10m DEMs (10m DEMS) by calculating the average value of each 2 by 2 grid in the 5m DEMs. The resolution-reduced 10m DEMs could generate some differences in the morphological analysis, but the expected scale of the landslide susceptibility in this study was set to 1:25,000, so differences smaller than 12.5m could be ignored according to the relationship between mapping scale and 5% acceptable error.

This study followed the method proposed by Xie et al. (2004) in delineating slope units according to gullies and ridges.

First, gullies and watersheds were analyzed by successively using spatial analysis tools in ArcGIS: fill, flow direction, flow accumulation, stream link (with 2,000 used as the threshold) and watershed. Second, reverse DEMs were generated by multiplying DEMs by -1. In the reverse DEMs, ridges became gullies and could be analyzed by the same methods used in the first step. Third, the watersheds of the DEMs and reverse DEMs were transformed from rasters to polygons for further editing by using the "Raster to Polygon" tool in ArcGIS and then cut by each other to delineate the slope units. Finally, slope units were modified manually according to aspect and gradient. It is suggested that the aspect in a slope unit should be within three adjacent directions; e.g., northwest, north, and northeast. On the other hand, the difference in gradient should not be over 30 degrees in a slope unit, and slope units situated on flat areas, including alluvial deposits and terraces, were deleted. In addition, the area of each slope unit was set to around 5 ha; therefore, slope units smaller than 5 ha were combined with adjacent slope units and those larger than 5 ha were split into several smaller ones. Moreover, slope units delineated by parallel drainage on a dip slope were combined into one slope unit. After the editing, each slope unit was given a unique code for disaster prevention.

### 3.4 **Landslide Susceptibility Factors**

Several predisposing factors that might lead to landslides were selected initially in this study to construct a landslide susceptibility model for slope units. These factors included rock mass strength-size classification (RMSSC I–VII), dip slope, average slope, variance of slope, ratio of steep slope, total slope height, average elevation, average curvature, variance of curvature, fault density, fold density, average wetness, rainfall intensity, total rainfall, 3-hour mean rainfall intensity ($I_3$), and 24-hour accumulated rainfall ($R_{24}$). The relationships of these factors to landslides could be analyzed through graphic discrimination, including success rate curve, probability of failure curve, and difference between landslide and non-landslide groups (Lee, 2014). After that, factor correlation analyses were applied to delete highly related factors to keep the factors used in the landslide susceptibility model as independent as possible (Table 2).

In terms of geological factors, the lithology of a location is essential for the analysis of landslide susceptibility. However, our study area had more than 50 detailed types of lithology, which was unfavorable for the analysis. Therefore, we adopted the 1:25,000 rock mass strength-size classification maps from Central Geological Survey, Taiwan, to replace the use of lithology (Franklin, 1975; Central Geological Survey, 2008). In addition, the dip slope inventory interpreted manually from 1:5,000 aerial photographs by the Central Geological Survey, Taiwan, was also adopted (Central Geological Survey, 2008). The fold density was also calculated by dividing the total length of all the folds by the total area in each slope unit.

For morphological factors, the average slope and the variance of slope were obtained by averaging and calculating the standard deviations of all the grid cells in the slope unit separately. In addition, shallow landslides are prone to occur on steep slopes; therefore, we also used the "ratio of steep slopes" to present how many steep slopes existed in a slope unit. It was found after trial and error that a threshold of gradient higher than 30 degrees had a higher relationship with landslide susceptibility. Thus, we calculated the area where the gradient was greater than 30 degrees ($A_{>30}$) as well as the total area ($A_{total}$) of each slope unit. Therefore, the ratio of steep slope could be calculated by dividing $A_{>30}$ by $A_{total}$. On the other hand, the average curvature and variance of curvature could also be calculated by the same method as slope in the ArcGIS software. The average wetness was calculated by averaging the wetness index of grid cells in a slope unit. This factor represents the effect of morphology on soil wetness. When the drainage area is larger and the slope is gentler, the water content in the soil will also be higher and therefore make a slope more prone to failure. The wetness index can be calculated according to the method proposed by Wilson and Gallant (2000) as follows:

$$\omega = ln(\frac{A_s}{tan\,\theta}) \tag{1}$$

where $\omega$ is wetness index, $A_s$ is the drainage area of a specific grid cell, and $\theta$ is the slope of the grid.

For triggering factors, we collected hourly rainfall data of 423 rain stations provided by Central Weather Bureau, Taiwan (96 of which were located in our study area, shown in Fig. 1) and analyzed both the 3-hour mean rainfall intensity ($I_3$) and the 24-hour accumulated rainfall ($R_{24}$) of each station for each rainfall events in Table 2. After that, we used the linear mode of ordinary kriging and applied the default setting in Surfer software to obtain the rainfall distribution of the whole study area. Whenever Taiwan has a typhoon event, the Central Weather Bureau issues disaster prevention alerts. We therefore counted the time that the first alert was issued as the beginning of the rainfall event and the time that the alert was cancelled as the end of the rainfall event to calculate rainfall amounts. Our reasons for choosing 3-hour mean rainfall intensity ($I_3$) and 24-hour accumulated rainfall ($R_{24}$) as factors will be explained in detail in section 4.2.

## 4 Methodology

### 4.1 Landslide susceptibility analysis

The main purpose of landslide susceptibility analysis is to determine the effectiveness of each predisposing factor and the relative possibility of landslide occurrence in a specific area. Several methods can be used to analyze landslide susceptibility. The deterministic method uses a physical model and geotechnical material properties to determine the safety factor of slopes; however, precise parameters of materials are difficult to obtain, especially on a regional scale (Montgomery and Dietrich, 1994; Van Westen and Terlien, 1996). The qualitative and semi-quantitative methods rely on the experience and knowledge of the experts who carried out the analysis; however, these results might vary from one expert to another. The machine learning method uses multiple samples to build a model by trial and error; however, it is time consuming (Gorsevski and Jankowski, 2010; Yeon et al., 2010; Yilmaz, 2010; Marjanovic et al., 2011; Lee et al., 2012; Song et al., 2012). The statistical method also requires numerous samples for the training; however, it is more efficient, especially when dealing with regional-scale analyses, and can avoid the uncertainty of material parameters as well as differences in expert experience. Recently, nonlinear analysis, a statistical method, has been used for the analysis of complex landslide phenomena. Methods such as logistic regression (Yilmaz, 2010; Lee et al., 2012, 2014, 2015; Schlögel et al., 2017) and discriminant analysis (Lee et al., 2004, 2008a, 2008b) are often used to analyze landslide susceptibility. In this study, we applied logistic regression (LR) to evaluate the susceptibility of each slope unit (Guzzetti et al., 1999; Ayalew and Yamagishi, 2005). The LR function can be expressed as follows:

$$P = \frac{1}{1 + e^{-z}} \tag{2}$$

$$z = \sum_{i=1}^{m} L_i w_i + \sum_{j=1}^{n} F_j w_{m+j} + C \tag{3}$$

where $P$ is landslide susceptibility, $L_i$ is RMSSC factor ($L_{01}$ to $L_{07}$ in Table 2), $F_j$ is other factors ($F_{01}$ to $F_{10}$ in Table 2), $w_i$ and $w_{m+j}$ are regression coefficients, and $C$ is a constant. Six event-based landslide inventories in this study were used to label whether or not landslides occurred in the slope units. After that, all the slope units were divided randomly into two groups, one for training the model and the other for validation. The index indicating landslide/non-landslide was set as the dependent variable, and all the landslide susceptibility factors were set as covariates in SPSS for training of the model. After iterative training, the regression coefficients of each landslide susceptibility factor, as well as the success rate curve (SRC), the prediction rate curve (PRC), and the area under the curve (AUC), were reported in SPSS. The AUC can be used to examine if the model predicts landslides well, and the regression coefficients can be used for the prediction of landslide susceptibility. During the process of training, several details required attention. Because the non-landslide samples outnumbered the

landslide samples, we randomly selected equal numbers of non-landslide and landslide samples for the training so as to avoid the effect of difference in quantity. In addition, different samples could have led to different results when selecting non-landslide samples randomly. To reduce this effect, we prepared several sets of randomly-selected samples for the analysis of landslide susceptibility to test if the model was stable enough; i.e., the AUC would not vary severely when validating models with different sets of samples. Finally, the individual landslide susceptibilities of slope units were calculated with this model and classified into high, moderate and low susceptibility levels.

## 4.2 $I_3$–$R_{24}$ rainfall index and thresholds

Rainfall-induced landslides are triggered by either high intensity rainfall or high accumulated rainfall (Larsen and Simon, 1993; Corominas and Moya; 1999; Yu et al., 2006). To identify rainfall indexes responsible for landslides, the triggering rainfall, including the rainfall intensity ($I_1$, $I_2$, $I_3$, $I_4$, $I_5$, $I_6$) and accumulated rainfall ($R_6$, $R_{12}$, $R_{24}$, $R_{48}$, $R_{72}$) of different time windows of each landslide case were analyzed according to the landslide occurrence time. The results revealed that 218 landslides occurred within the 3 hours following the highest rainfall intensity, and 242 occurred within the 3 hours following the 2nd or 3rd highest rainfall intensity (i.e., induced by high rainfall intensity), accounting for nearly 49% of the landslide cases gathered in this study (Table 3). From these results, it became clear that in Taiwan, $I_3$ is the most important index for landslides induced by rainfall of short duration but high intensity. On the other hand, 481 landslides occurred close to the end of the rainfall events (i.e., induced by high accumulated rainfall), accounting for about 51% of the total cases. Furthermore, analysis of the different accumulated rainfall indexes showed that 24-hour accumulated rainfall had the lowest coefficient of variation (Table 4), indicating that this index was less dispersive than others and might be more suitable for serving as an accumulated rainfall index for establishing rainfall thresholds. The coefficient of variation can be calculated as follows:

$$C_v = \frac{\sigma}{\mu} \tag{4}$$

where $C_v$ is the coefficient of variation, and $\sigma$ and $\mu$ are the standard deviation and average of accumulated rainfall of all the cases used in this study respectively.

Based on these data and previous studies (Cheung et al., 2006; Liao et al., 2010), 3-hour mean rainfall intensity ($I_3$) and 24-hour accumulated rainfall ($R_{24}$) were respectively chosen as the short-term and long-term rainfall indexes for the establishment of the rainfall threshold (Fig. 3). We chose 3-hour mean rainfall intensity here instead of 3-hour accumulated rainfall to focus on rainfall of short duration but high intensity. Similarly, we chose 24-hour accumulated rainfall to focus on rainfall of long duration but low intensity. Finally, rainfall thresholds were decided by plotting the $I_3$ and $R_{24}$ rainfall index of historical landslides in the $I_3$–$R_{24}$ diagram (Fig. 4). Here we used the ellipse as the threshold line, and the parameters $a$ (semi-major axis) and $b$ (semi-minor axis) of the ellipse were set according to the slope of best fit line obtained from the least square method. Thresholds such as 90%, 60%, 30%, 15% were determined according to the percentage of historical cases that could be enveloped under the threshold line; e.g., the 90% threshold ($T_{90\%}$) included 90% of the historical cases. A higher threshold indicates a more dangerous condition for the occurrence of landslides. The original warning values of $I_3$ and $R_{24}$ of the 90%, 60%, 30%, 15% thresholds were equal to the semi-minor axis and semi-major axis of each threshold respectively. After that, $I_3$ was rounded to the nearest 5 mm/h and $R_{24}$ was rounded to the nearest 50 mm for operational purposes, such as the evacuation of residents.

## 4.3 **Landslide early warning model and validation**

The landslide early warning model in this study considered both landslide susceptibility and rainfall thresholds and alerts were determined by using a hazard matrix. As mentioned above, the LR method was applied to analyze the susceptibility of each slope unit. After that, all the slope units were categorized into high, moderate, and low susceptibility levels. We consequently established rainfall thresholds for each susceptibility level separately and then set alerts of red, orange, yellow and green according to the level of danger.

High-susceptibility slopes might be more susceptible to rainfall. Hence, the alerts were set as red (extreme danger level) for rainfall conditions exceeding the 60% threshold line, orange (high danger level) for those between the 60% and 30% threshold lines, yellow (medium danger level) for those between the 30% and 15% threshold lines, and green (low danger level) for rainfall conditions lower than the 15% threshold line (Fig. 5). For moderate-susceptibility slopes, the alerts were set as red for rainfall conditions exceeding the 90% threshold line, orange for those between the 90% and 60% threshold lines, yellow for rainfall conditions between the 60% and 30% threshold lines, and green for rainfall conditions lower than the 30% threshold line. Low-susceptibility slopes should be less susceptible to rainfall. Hence, the alerts were set as orange for rainfall conditions exceeding the 90% threshold line, yellow for those were between the 90% and 60% threshold lines, and green for those lower than the 60% threshold line.

Several methods can be used for the validation of a landslide early warning model (Segoni et al., 2014, 2018; Gariano, 2015; Rosi et al, 2015; Piciullo et al., 2017; Krøgli et al., 2018). According to the analysis of Segoni et al. (2018), compiling a contingency matrix and calculating skill scores is the most commonly used method in recent years. Therefore, we applied this method and quantitatively validated our model with probability of detection (POD, also known as hit rate), probability of false detection (POFD, also known as false alarm rate) and probability of false alarm (POFA, also known as false alarm ratio). The contingency matrix is presented as Table 5. Comparing the observed events and the forecasted events produces four outcomes: True Positive (TP), True Negative (TN), False Positive (FP) and False Negative (FN). Because in Taiwan, warnings of natural hazards are always issued by taking a village as a unit, here we validated our model on the village scale. TP indicated the number of villages for which warnings of slope units were issued and landslides did occur, while TN indicated the number of villages for which no warning was issued and no landslide occurred. On the other hand, FP indicated the number of villages for which warnings were issued but no landslides occurred, also known as false alarms, while FN indicated the number of villages for which no warnings were issued but landslides did occur; i.e., missed alarms. In addition, in our study, we defined red (extreme danger level) and orange (high danger level) alerts as warnings issued for evacuation; i.e., the alarm zone in our model. On the other hand, yellow (medium danger level) and green (low danger level) alerts were considered to indicate no need for evacuation; i.e., the no alarm zone in our model. POD, POFD, POFA can be calculated by the following equations:

$$POD = \frac{TP}{TP+FN} \tag{5}$$

$$POFD = \frac{FP}{TP+FP} \tag{6}$$

$$POFA = \frac{FP}{FP+TN} \tag{7}$$

The ranges of POD, POFD, POFA are all between 0 to 1, and their optimal values are 1, 0 and 0, respectively.

## 5 Results and discussions

### 5.1 Landslide susceptibility analysis

After several calibrations, the resultant model was obtained. The coefficients for each factor of LR are given in Table 2, and the landslide susceptibility of each slope unit was also calculated. To evaluate the quality of a predicted model, the success rate curve (SRC) and prediction rate curve (PRC) (Chung and Fabbri, 1999) were mapped, and then the area under the curve (AUC) was used to describe the model's ability to distinguish landslide and non-landslide (Yesilnacar and Topal, 2005). A higher AUC value indicated a better model for the prediction of landslides. If the AUC value was 0.5, it meant that the model did not predict the occurrence of the landslide better than a random approach. If the AUC value was 1.0, the capability of the model for predicting a landslide was perfect.

In our study, the AUCs were 0.745 and 0.691 in training and validation respectively, indicating that our LR model could identify 60% of the landslides in the top 25% and 30% of the highest susceptibility areas during training and validation (Fig. 6). These results showed that the LR model was acceptable in both the training and the validation. For a statistical landslide susceptibility analysis, it is essential to use as many samples as possible. However, we used slope units instead of grid units in this study for application to disaster prevention. This led to the reduction of samples, since one slope unit might equal hundreds of grids. Therefore, our AUC might not be considered high in comparison to a grid-based landslide susceptibility model.

On the other hand, to avoid over-training, it was necessary to validate the capability of the model. One common method is to divide the study area into sub-regions such as left and right, one for training and the other for validation (Chung and Fabbri, 2008). But this method might cause the loss of a training pattern in a small or particular geological region if the study area is extensive. To overcome this problem, we used multi-event data from the same area for training and testing. The data used in this study were therefore randomly divided into two portions, and several sets of data were tested. This approach would also solve the problems mentioned above.

### 5.2 $I_3$–$R_{24}$ rainfall threshold

We gathered a total of 941 landslide cases in this study and used 240 cases located in southern Taiwan, consisting of 110 high-susceptibility cases, 84 moderate-susceptibility cases, and 46 low-susceptibility cases, to establish a susceptibility-based regional landslide early warning model. The ellipse-shaped $I_3$–$R_{24}$ rainfall thresholds for 3 different landslide susceptibility slopes are presented in Fig. 7. For practical use, the original threshold values of $I_3$ and $R_{24}$ (as shown in the parentheses in Fig. 8) were separately rounded to the nearest 5 mm/h and the nearest 50 mm. It was found that the threshold values gradually increased as the susceptibility of slope units decreased for the same alert level, indicating that greater rainfall amounts would be needed when issuing alters on less susceptible slope units. These results showed that establishing rainfall thresholds according to different landslide susceptibilities and then setting alert levels by adopting a hazard matrix not only provided differentiated thresholds but also avoided the over- or underestimation of the thresholds for slopes.

After the establishment of the landslide early warning model, we converted the model to an early warning system (EWS) connected to the QPESUMS, which provides nearly real-time radar rainfall data, for disaster prevention. Based on the alerts present in the system, the corresponding danger levels and suggested actions for residents around the warning slope are shown in Table 6. During a yellow alert, residents should listen for further announcements and prepare for evacuation if the alert is raised to orange. When an orange alert is issued, residents should evacuate as quickly as possible because landslides are likely to occur, according to the validations shown in the next section. Finally, when a red alert is issued, evacuation may need to be

enforced to protect residents from injury.

### 5.3 **Validation of landslide early warning model**

We validated our model with two kinds of data: (1) three disastrous shallow landslides in 2016 and the occurrence times provided by witnesses; (2) a landslide inventory of two historical typhoon events and the occurrence times reported by newspapers.

The first set of validation data showed that orange or red alerts could have been issued in advance for all of the disastrous landslides before the landslides occurred, according to the rainfall snake line in the $I_3$–$R_{24}$ diagram (Fig. 9; Table 7).

The Shihwen landslide occurred on a low-susceptibility slope. From the rainfall histogram and $I_3$–$R_{24}$ diagram (Fig. 9(a)), we knew that the occurrence time was quite close to the end of the rainfall event, and that the $I_3$ was only 2.3 mm/h while the $R_{24}$ was 507.5 mm, indicating that accumulated rainfall might have been the principal cause of this case. The rainfall snake line showed that on September 14, the alert was raised to yellow at 10:00 and then to orange at 11:00 during the downpour. Then the precipitation fell for several hours, and the alert was lowered to yellow. However, when it rained again, the alert was raised back to orange at 18:00 and at 23:00, and the landslide occurred at 05:00 on September 15.

The Zhongmin landslide occurred on a high-susceptibility slope. From the rainfall histogram and $I_3$–$R_{24}$ diagram (Fig. 9(b)), it was found that the occurrence time was also quite close to the end of the rainfall event and that the $I_3$ was 8.3 mm/h while the $R_{24}$ was 479 mm. The high rainfall intensity (74 mm/h at 04:00 on September 28) and accumulated rainfall might both have contributed to this case. The rainfall snake line showed that on September 28, the yellow alert was raised to orange and red at 04:00 during the high intensity rainfall mentioned above. After that, although the rainfall soon fell off, the landslide occurred 6 hours later, at 10:00 on September 28, during an orange alert.

The Houcuo landslide also occurred on a low-susceptibility slope. From the rainfall histogram and $I_3$–$R_{24}$ diagram (Fig. 9(c)), we found that the occurrence time was close to time that the highest rainfall intensity showed in the rainfall event, and the $I_3$ was 24.3 mm/h while the $R_{24}$ was 291.3 mm, indicating that high rainfall intensity might have been responsible for this case. Due to this intensity, the rainfall snake line showed that the alert was raised from green to yellow and then to orange within just one hour, from 03:00 to 04:00, on September 28, and the landslide occurred at around 03:30.

For the second set of validation data, we applied the kriging method to interpolate spatial rainfall data and analyzed the alerts for each slope unit hour-by-hour. The results showed that the hit rates in the two historical typhoon events were all sufficiently high, according to the accumulative warning numbers relative to the numbers of landslide slopes (Fig. 10; Table 8).

During Typhoon Mindulle in 2004, landslides occurred in 10,911 slope units, including 5,129 high-susceptibility slopes, 2,750 moderate-susceptibility slopes and 3,032 low-susceptibility slopes. According to newspaper reports, several landslides occurred at 10:00 and between 15:00 and 16:00 on July 2, 2004; however, most of the landslides occurred between 06:00 and 13:00 the next day, July 3, 2004 (blue dashed box in Fig. 10(a)). From the alert history (Fig. 10(a)), it was found that the peak number of orange and red alerts matched the reported occurrence times quite well. In addition, orange alerts, indicating the need for evacuation, had been issued for 8,283 slope units during the whole event, accounting for 75.9% of the slope units where landslides occurred in this event.

Typhoon Haitang in 2005 was another event of concern. Landslides occurred in 10,804 slope units, including 2,592 high-susceptibility slopes, 2,355 moderate-susceptibility slopes and 5,857 low-susceptibility slopes. According to newspaper reports, landslides occurred between 05:00 on July 19 and 06:00 on July 20, 2005 (blue dashed box in Fig. 10(b)). From the alert history (Fig. 10(b)), it was found that landslides occurred immediately after the number of orange and red alerts increased

sharply, and the peak number of orange and red alerts also matched the reported occurrence times quite well. On the other hand, orange alerts had been issued for 10,245 slope units during the whole event, accounting for 94.8% of the slope units where landslides occurred in this event. These results revealed that our model could provide valuable information for evacuation and disaster prevention.

5      In addition, the second set of validation data was also used to validate the warnings issued for villages during two typhoon events by adopting the contingency matrix and skill scores. According to the event-based landslide inventories, if any landslides were located in a village, the village was classified as "Yes" for observed events. If orange or red warning alerts were issued for slope units in a village, the village was classified as "Yes" for forecasted events. Based on these rules, the numbers of True Positive (TP), True Negative (TN), False Positive (FP) and False Negative (FN) were counted and the skill

10 scores were calculated (Table 9). The probabilities of detection (PODs) of the two typhoon events were 0.961 and 0.874 respectively, indicating that most of the villages where landslides occurred could have been warned in advance. The probabilities of false detection (POFDs) of the two typhoon events were 0.280 and 0.667 respectively, suggesting that the model performed well for Typhoon Mindulle but might not be so ideal for Typhoon Haitang. Lastly, the probabilities of false alarm (POFAs) of the two typhoon events were 0.120 and 0.110 respectively, which meant that our model would not issue an

15 excessive number of false alarms and was feasible for disaster prevention.

## 6 Conclusions

This study attempted to establish regional rainfall thresholds for shallow landslides according to their landslide susceptibility levels and set alerts with a hazard matrix to provide more detailed results for disaster mitigation.

     Logistic Regression (LR), a statistical method, was applied in this study to analyze the landslide susceptibilities of slope

20 units. The areas under the curve (AUC) were 0.745 and 0.691 in the training and validation respectively. Due to our use of slope units instead of grid units in this study for application to disaster prevention, the number of our training samples was less, since one slope unit might equal hundreds of grids. Therefore, our AUC might not be considered high as compared to a grid-based landslide susceptibility model, but it was still acceptable for practical use.

     This study also examined the relationships between rainfall indexes and the occurrence of landslides. From 941 landslide

25 cases we gathered, it was found that 3-hour mean rainfall intensity ($I_3$) and 24-hour accumulated rainfall ($R_{24}$) were the most dominant short-term and long-term parameters responsible for rainfall-induced landslides in Taiwan. There were 460 cases (about 49%) occurred within the 3 hours following the highest, 2nd and 3rd rainfall intensities, while 24-hour accumulated rainfall had the lowest coefficient of variation of the long-term rainfall indexes. The $I_3$-$R_{24}$ rainfall index was therefore used to establish rainfall thresholds.

30      We categorized the slope units into 3 landslide susceptibility levels (high, moderate, low) and then separately established a susceptibility-based regional rainfall threshold. We also set three alert levels, including red (extreme danger level), orange (high danger level), and yellow (medium danger level), by adopting a hazard matrix for application to evacuation decisions. It was found that the threshold values gradually increased as the susceptibility of slope units decreased for the same alert level, indicating that greater rainfall amounts would be needed when issuing alters on less susceptible slope units.

35      Validations using three disastrous shallow landslides in 2016 and two landslide inventories of historical typhoon events showed that, for the landslide cases in 2016, orange or red alerts could have been issued before the landslides occurred and the hit rates of the alerts issued for slope units in the two historical typhoon events were 75.9% and 94.8% respectively, which are sufficiently high for a landslide early warning model. In addition, the skill scores applied to the validation of alerts issued for villages during two typhoon events showed that the probabilities of detection (PODs) were 0.961 and 0.874, the probabilities

of false detection (POFDs) were 0.280 and 0.667, and the probabilities of false alarm (POFAs) were 0.120 and 0.110 respectively, indicating that our model could be used for landslide early warnings.

It can concluded that classifying landslide susceptibility and establishing rainfall thresholds separately not only provides refined thresholds but also avoids over- or underestimation of the thresholds for slopes, especially when considering the application to disaster prevention.

**Acknowledgements**

The authors would like to thank the Central Geological Survey, Taiwan, for supporting this research financially and for providing helpful comments on the research.

**References**

1. Ayalew, L.: The effect of seasonal rainfall on landslides in the highlands of Ethiopia, B Eng Geol Environ, 58(1), 9–19, 1999. https://doi.org/10.1007/s100640050065

2. Bell, F. G., and Maud, R. R.: Landslides associated with the colluvial soils overlying the Natal Group in the greater Durban region of Natal, South Africa, Environ Geol, 39(9), 1029–1038, 2000. https://doi.org/10.1007/s002549900077

3. Brunetti, M. T., Peruccacci, S., Rossi, M., Luciani, S., Valigi, D., and Guzzetti, F.: Rainfall thresholds for the possible occurrence of landslides in Italy, Nat. Hazards Earth Syst. Sci.,Sci., 10(3), 447–458, 2010. https://doi.org/10.5194/nhess-10-447-2010

4. Caine, N.: The rainfall intensity-duration control of shallow landslides and debris flows, Geogr Ann A, 62, 23–27, 1980. https://doi.org/10.1080/04353676.1980.11879996

5. Calvello, M., d'Orsi, R. N., Piciullo, L., Paes, N., Magalhaes, M. and Lacerda, W. A.: The Rio de Janeiro early warning system for rainfall-induced landslides: analysis of performance for the years 2010–2013, International journal of disaster risk reduction, 12, 3–15, 2015. https://doi.org/10.1016/j.ijdrr.2014.10.005

6. Carrara, A.: Drainage and divide networks derived from high-fidelity digital terrain models, Quantitative Analysis of Mineral and Energy Resources, in: Quantitative analysis of mineral and energy resources, Springer, Dordrech, 581–597, 1988. https://doi.org/10.1007/978-94-009-4029-1_34

7. Carrara, A., and Guzzetti, F.: GIS Technology in Mapping Landslide Hazard, in: Geographical information systems in assessing natural hazards, Springer, Netherlands, 135–175, 1995. https://doi.org/10.1007/978-94-015-8404-3_8

8. Carrara, A., Cardinali, M., Detti, R., Guzzetti, F., Pasqui, V., and Reichenbach, P.: GIS Techniques and statistical models in evaluating landslide hazard, Earth Surf Proc Land, 16(5), 427–445, 1991. https://doi.org/10.1002/esp.3290160505

9. Central Geological Survey: Enviromental-Geological Database in Slopeland of Urban Area, 2008. (in Chinese)

10. Chen, H., Lin, G. W., Lu, M. H., Shih, T. Y., Horng, M. J., Wu, S. J. and Chuang, B.: Effects of topography, lithology, rainfall and earthquake on landslide and sediment discharge in mountain catchments of southeastern Taiwan, Geomorphology, 133(3-4), 132-142, 2011. https://doi.org/10.1016/j.geomorph.2010.12.031

11. Cheung, S. P. Y., Wong, M. C., and Yeung, L. H. Y.: Application of rainstorm nowcast to real-time warning of landslide hazards in Hong Kong, in: WMO PWS Workshop on Warnings of Real-Time Hazards by Using Nowcasting Technology, Sydney, Australia, 1–21, 2006.

12. Chung, C. J., and Fabbri, A. G.: Predicting landslides for risk analysis - spatial models tested by a cross-validation technique,, Geomorphology, 94(3), 438–452, 2008. https://doi.org/10.1016/j.geomorph.2006.12.036

13. Corominas, J., and Moya, J.: Reconstructing recent landslide activity in relation to rainfall in the Llobregat River basin, Eastern Pyrenees, Spain,, Geomorphology, 30(1), 79–93, 1999. https://doi.org/10.1016/S0169-555X(99)00046-X

14. Dadson, S. J., Hovius, N., Chen, H., Dade, W. B., Hsieh, M. L., Willett, S. D., Hu, J. C., Horng, M. J., Chen, M. C., Stark, C. P., Lague, D. and Lin, J. C.: Links between erosion, runoff variability and seismicity in the Taiwan orogen, Nature, 426(6967), 648, 2003. https://doi.org/10.1038/nature02150

15. Devoli, G., Kleivane Krøgli, I., Dahl, M. P., Colleuille, H., Nykjær Boje, S. and Sund, M.: Geoethical considerations in early warning of flooding and landslides: Case study from Norway, EGU General Assembly, 2015.

16. Evans, S. G., Guthrie, R. H., Roberts, N. J., and Bishop, N. F.: The disastrous 17 February 2006 rockslide-debris avalanche on Leyte Island, Philippines: a catastrophic landslide in tropical mountain terrain, Nat. Hazards Earth Syst. Sci.,. 7(1), 89–101, 2007. https://doi.org/10.5194/nhess-7-89-2007

17. Fan, X., Xu, Q., Scaringi, G., Dai, L., Li, W., Dong, X., Zhu, X., Pei, X., Dai, K., and Havenith, H. B.: Failure mechanism and kinematics of the deadly June 24th 2017 Xinmo landslide, Maoxian, Sichuan, China, Landslides, 14(6), 2129–2146, 2017. https://doi.org/10.1007/s10346-017-0907-7

18. Franklin, J. A.: Safety and Enconomy in Tunneling, in: Proc. 10th Can. Rock Mech. Symp, Queens University, Kingston, Canada, 325–341, 1975.

19. Gariano, S. L., Brunetti, M. T., Iovine, G., Melillo, M., Peruccacci, S., Terranova, Terranova, O., Vennari, C., and Guzzetti, F.: Calibration and validation of rainfall thresholds for shallow landslide forecasting in Sicily, southern Italy, Geomorphology, 228, 653–665, 2015. https://doi.org/10.1016/j.geomorph.2014.10.019

20. Gorsevski, P. V., and Jankowski, P.: An optimized solution of multicriteria evaluation analysis of landslide susceptibility using fuzzy sets and Kalman filter, Comput Geosci, 36(8), 1005–1020, 2010. https://doi.org/10.1016/j.cageo.2010.03.001

21. Guzzetti, F., Carrara, A., Cardinali, M., and Reichenbach, P.: Landslide hazard evaluation: a review of current techniques and their application in a multi-scale study, Central Italy, Geomorphology, 31(1), 181–216, 1999. https://doi.org/10.1016/S0169-555X(99)00078-1

22. Guzzetti, F., Peruccacci, S., Rossi, M., and Stark, C. P.: The rainfall intensity-duration control of shallow landslides and debris flows: an update, Landslides, 5(1), 3–17, 2008. https://doi.org/10.1007/s10346-007-0112-1

23. Guzzetti, F., Peruccacci, S., Rossi, M., and Stark, C. P.: Rainfall thresholds for the initiation of landslides in central and southern Europe,, Meteorol Atmos Phys, 98(3-4), 239–267, 2007. https://doi.org/10.1007/s00703-007-0262-7

24. Guzzetti, F., Mondini, A. C., Cardinali, M., Fiorucci, F., Santangelo, M., and Chang, K. T.: Landslide inventory maps: New tools for an old problem. Earth-Sci Rev, 112(1), 42–66, 2012. https://doi.org/10.1016/j.earscirev.2012.02.001

25. Hong, Y., Hiura, H., Shino, K., Sassa, K., Suemine, A., Fukuoka, H. and Wang, G.: The influence of intense rainfall on the activity of large-scale crystalline schist landslides in Shikoku Island, Japan, Landslides, 2(2), 97–105, 2005. https://doi.org/10.1007/s10346-004-0043-z

26. Hong, Y., and Adler, R. F.: Predicting global landslide spatiotemporal distribution: integrating landslide susceptibility zoning techniques and real-time satellite rainfall estimates, Int J Sediment Res, 23(3), 249–257, 2008. https://doi.org/10.1016/S1001-6279(08)60022-0

27. Iverson, R. M., George, D. L., Allstadt, K., Reid, M. E., Collins, B. D., Vallance, J. W., Schilling, S. P., Godt, J. W., Cannon, C. M., Magirl, C. S., Baum, R. L., Coe, J. A., Schulz, W. H., and Bower, J. B.: Landslide mobility and hazards: implications of the 2014 Oso disaster, Earth Planet Sc Lett , 412, 197–208, 2015. https://doi.org/10.1016/j.epsl.2014.12.020

28. Kim, D., Im, S., Lee, S. H., Hong, Y., and Cha, K. S.: Predicting the rainfall-triggered landslides in a forested mountain region using TRIGRS model, J Mt Sci, 7(1), 83–91, 2010. https://doi.org/10.1007/s11629-010-1072-9

29. Krøgli, I. K., Devoli, G., Colleuille, H., Sund, M., Boje, S. and Engen I. K.: The Norwegian forecasting and warning

service for rainfall-and snowmelt-induced landslides, Nat. Hazards Earth Syst. Sci. Discuss., 2017. https://doi.org/10.5194/nhess-2017-426

30. Larsen, M. C., and Simon, A.: A rainfall intensity-duration threshold for landslides in a humid-tropical environment, Puerto Rico, Geografiska Annaler, Series A, Phys Geogr, 13–23, 1993. https://doi.org/10.1080/04353676.1993.11880379

31. Lee, C. T.: Statistical Seismic Landslide Hazard Analysis: An Example from Taiwan, Eng Geol, 182, 201–212, 2014. https://doi.org/10.1016/j.enggeo.2014.07.023

32. Lee, C. T., Huang, C. C., Lee, J. F., Pan, K. L., Lin, M. L., and Dong, J. J.: Statistical Approach to Earthquake-Induced Landslide Susceptibility,, Eng Geol, 100(1-2), 43–58, 2008a. https://doi.org/10.1016/j.enggeo.2008.03.004

33. Lee, C. T., Huang, C. C., Lee, J. F., Pan, K. L., Lin, M. L., and Dong, J. J.: Statistical approach to storm event-induced landslide susceptibility, Nat. Hazards Earth Syst. Sci.,. 8(4), 941–960, 2008b. https://doi.org/10.5194/nhess-8-941-2008

34. Lee, C. T., Huang, C. C., Lee, J. F., Pan, K. L., Lin, M. L., Liao, C. W., Lin, P. S., Lin, Y. S., Chang, C. W.: Landslide susceptibility analyses based on three different triggering events and result comparison, in: Proceeding of International Symposium on Landslide and Debris Flow Hazard Assessment, 6, 1–18, 2004.

35. ,M. J., Choi, J. W., Oh, H. J., Won, J. S., Park, I. and Lee, S.: Ensemble based landslide susceptibility maps in Jinbu area, Korea, Environ Earth Sci, 67(1), 23-37, 2012. https://doi.org/10.1007/978-3-642-25495-6_7

36. Lee, S., Won, J. S., Jeon, S. W., Park, I., and Lee, M. J.: Spatial landslide hazard prediction using rainfall probability and a logistic regression model, Math Geosci, 47(5), 565–589, 2015. https://doi.org/10.1007/s11004-014-9560-z

37. Liao, Z., Hong, Y., Wang, J., Fukuoka, H., Sassa, K., Karnawati, D., and Fathani, F.: Prototyping an experimental early warning system for rainfall-induced landslides in Indonesia using satellite remote sensing and geospatial datasets, Landslides, 7(3), 317–324, 2010. https://doi.org/10.1007/s10346-010-0219-7

38. Lin, G. W., Chen, H., Hovius, N., Horng, M. J., Dadson, S., Meunier, P. and Lines, M.: Effects of earthquake and cyclone sequencing on landsliding and fluvial sediment transfer in a mountain catchment, Earth Surf. Proc. Land., 33(9), 1354-1373, 2008. https://doi.org/10.1002/esp.1716

39. Luo, W., and Liu, C. C.: Innovative landslide susceptibility mapping supported by geomorphon and geographical detector methods, Landslides, 15(3), 465–474474, 2017. https://doi.org/10.1007/s10346-017-0893-9

40. Marjanović, M., Kovačević, M., Bajat, B., and Voženílek, V.: Landslide susceptibility assessment using SVM machine learning algorithm, Eng Geol, 123(3), 225–234, 2011. https://doi.org/10.1016/j.enggeo.2011.09.006

41. Martelloni, G., Segoni, S., Fanti, R., and Catani, F.: Rainfall thresholds for the forecasting of landslide occurrence at regional scale, Landslides, 9(4), 485–495, 2011. https://doi.org/10.1007/s10346-011-0308-2

42. Montgomery, D. R., and Dietrich, W.E.: A physical-based model for the topographic control on shallow landsliding, Water Resour Res, 30(4), 1153–1171, 1994. https://doi.org/10.1029/93WR02979

43. Osanai, N., Shimizu, T., Kuramoto, K., Kojima, S., and Noro, T.: Japanese early-warning for debris flows and slope failures using rainfall indices with Radial Basis Function Network, Landslides, 7(3), 325–338, 2010. https://doi.org/10.1007/s10346-010-0229-5

44. Petley, D.: Global patterns of loss of life from landslides, Geology, 40(10), 927–930, 2012. https://doi.org/10.1130/G33217.1

45. Peruccacci, S., Brunetti, M. T., Gariano, S. L., Melillo, M., Rossi, M., and Guzzetti, F.: Rainfall thresholds for possible landslide occurrence in Italy, Geomorphology, 290, 39–57, 2017. https://doi.org/10.1016/j.geomorph.2017.03.031

46. Piciullo, L., Dahl, M. P., Devoli, G., Colleuille, H., and Calvello, M.: Adapting the EDuMaP method to test the performance of the Norwegian early warning system for weather-induced landslides, Nat. Hazards Earth Syst. Sci., 17, 817-831, 2017. https://doi.org/10.5194/nhess-17-817-2017

47. Pradhan, A. M. S., Kang, H. S., Lee, J. S., and Kim, Y. T.: An ensemble landslide hazard model incorporating rainfall threshold for Mt. Umyeon, South Korea, B Eng Geol Environ, online first, 2017. https://doi.org/10.1007/s10064-017-1055-y

48. Pumo, D., Conti, F. L., Viola, F., & Noto, L. V. (2017). An automatic tool for reconstructing monthly time-series of hydro-climatic variables at ungauged basins, Environmental Modelling & Software, 95, 381-400. https://doi.org/10.1016/j.envsoft.2017.06.045

49. Rosi, A., Segoni, S., Catani, F., and Casagli, N.: Statistical and environmental analyses for the definition of a regional rainfall threshold system for landslide triggering in Tuscany (Italy), J Geogr Sci, 22(4), 617-629, 2012. https://doi.org/10.1007/s11442-012-0951-0

50. Rosi, A., Lagomarsino, D., Rossi, G., Segoni, S., Battistini, A., and Casagli, N.: Updating EWS rainfall thresholds for the triggering of landslides,, Nat. Hazards, 78(1), 297–308, 2015. https://doi.org/10.1007/s11069-015-1717-7

51. Rosi, A., Peternel, T., Jemec-Auflič, M., Komac, M., Segoni, S., and Casagli, N.: Rainfall thresholds for rainfall-induced landslides in Slovenia, Landslides, 13(6), 1571-1577, 2016. https://doi.org/10.1007/s10346-016-0733-3

52. Rossi, M., Luciani, S., Valigi, D., Kirschbaum, D., Brunetti, M. T., Peruccacci, S., and Guzzetti, F.: Statistical approaches for the definition of landslide rainfall thresholds and their uncertainty using rain gauge and satellite data, Geomorphology, 285, 16–27, 2017. https://doi.org/10.1016/j.geomorph.2017.02.001

53. Samia, J., Temme, A., Bregt, A., Wallinga, J., Guzzetti, F., Ardizzone, F., and Rossi, M.: Do landslides follow landslides? Insights in path dependency from a multi-temporal landslide inventory, Landslides, 14(2), 547–558, 2017. https://doi.org/10.1007/s10346-016-0739-x

54. Sassa, K., Tsuchiya, S., Fukuoka, H., Mikos, M., and Doan, L.: Landslides: review of achievements in the second 5-year period (2009–2013), Landslides, 12(2), 213–223, 2015. https://doi.org/10.1007/s10346-015-0567-4

55. Schlögel, R., Marchesini, I., Alvioli, M., Reichenbach, P., Rossi, M., and Malet, J. P.: Optimizing landslide susceptibility zonation: Effects of DEM spatial resolution and slope unit delineation on logistic regression models, Geomorphology, 301301, 10–20, 2017. https://doi.org/10.1016/j.geomorph.2017.10.018

56. Segoni, S., Rosi, A., Rossi, G., Catani, F., and Casagli, N.: Analysing the relationship between rainfalls and landslides to define a mosaic of triggering thresholds for regional-scale warning systems, Nat. Hazards Earth Syst. Sci.,. 14(9), 2637, 2014. https://doi.org/10.5194/nhess-14-2637-2014

57. Segoni, S., Lagomarsino, D., Fanti, R., Moretti, S., and Casagli, N.: Integration of rainfall thresholds and susceptibility maps in the Emilia Romagna (Italy) regional-scale landslide warning system, Landslides, 12(4), 773–785, 2015. https://doi.org/10.1007/s10346-014-0502-0

58. Segoni, S., Piciullo, L. and Gariano, S. L.: A review of the recent literature on rainfall thresholds for landslide occurrence, Landslides, online first, 2018. https://doi.org/10.1007/s10346-018-0966-4

59. Song, K. Y., Oh, H. J., Choi, J., Park, I., Lee, C., and Lee, S.: Prediction of landslide using ASTER imagery and data mining models, Adv Space Res, 49, 978–993, 2012. https://doi.org/10.1016/j.asr.2011.11.035

60. Terlien, M. T.: The determination of statistical and deterministic hydrological landslide-triggering thresholds, Eng Geol, 35(2-3), 124–130, 1998. https://doi.org/10.1007/s002540050299

61. Tsou, C. Y., Feng, Z. Y., and Chigira, M.: Catastrophic landslide induced by typhoon Morakot, Shiaolin, Taiwan, Geomorphology, 127(3), 166–178, 2011. https://doi.org/10.1016/j.geomorph.2010.12.013

62. Turkington, T., Ettema, J., van Westen, C. J. and Breinl, K.: Empirical atmospheric thresholds for debris flows and flash floods in the Southern French Alps, Nat. Hazards Earth Syst. Sci.,. 14, 1517–1530, 2014. https://doi.org/10.5194/nhess-14-1517-2014

63. Valenzuela, P., Domínguez-Cuesta, M. J., García, M. A. M., and Jiménez-Sánchez, M.: A spatio-temporal landslide inventory for the NW of Spain: BAPA database, Geomorphology, 293, 11–23, 2017. https://doi.org/10.1016/j.geomorph.2017.05.010

64. Van Westen, C. J., and Terlien, M. T. J.: An approach towards deterministic landslide hazard analysis in GIS: A case study from Manizales (Colombia), Earth Surf Proc Land, 21, 853–868, 1996. https://doi.org/10.1002/(SICI)1096-9837(199609)21:9<853::AID-ESP676>3.0.CO;2-C

65. Van Westen, C. J., Rengers, N., and Soeters, R.: Use of geomorphological information in indirect landslide susceptibility assessment, Nat. Hazards, 30(3), 399–419, 2003. https://doi.org/10.1023/B:NHAZ.0000007097.42735.9e

66. Varnes, D. J.: Slope motion types and processes. In: Schuster, R.L., Krizek, R.J. (Eds.), Landslides, Analysis and Control, Special Report 176, Transportation Re-search Board, National Academy of Sciences, Washington, DC, 11–33, 1978.

67. Vessia, G., Parise, M., Brunetti, M. T., Peruccacci, S., Rossi, M., Vennari, C. and Guzzetti, F.: Automated reconstruction of rainfall events responsible for shallow landslides. Nat. Hazards Earth Syst. Sci.,. 14(9), 2399–2408, 2014. https://doi.org/10.5194/nhess-14-2399-2014

68. Wang, F., Wu, Y. H., Yang, H., Tanida, Y., and Kamei, A.: Preliminary investigation of the 20 August 2014 debris flows triggered by a severe rainstorm in Hiroshima City, Japan, Geoenvironmental Disasters, 2(1), 17, 2015. https://doi.org/10.1186/s40677-015-0025-6

69. Wilson, J. P. and Gallant, J. C.: Terrain analysis: principles and applications, John Wiley & Sons, Inc., 2000. ISBN:9780471321880

70. Xie, M., Esaki, T. and Zhou, G.: GIS-based probabilistic mapping of landslide zazard using a three-dimensional deterministic model, Nat. Hazards, 33(2), 265–282, 2004. https://doi.org/10.1023/B:NHAZ.0000037036.01850.0d

71. Yang, S. R.: Assessment of Rainfall-Induced Landslide Susceptibility Using GIS-Based Slope Unit Approach, J Perform Constr Fac, 31(4), 04017026, 2017. https://doi.org/10.1061/(ASCE)CF.1943-5509.0000997

72. Yang, H. and Adler, R. F.: Predicting global landslide spatiotemporal distribution: integrating landslide susceptibility zoning techniques and real-time satellite rainfall estimates, International Journal of Sediment Research, 23(3), 249-257, 2008. https://doi.org/10.1016/S1001-6279(08)60022-0

73. Yeon, Y. K., Han, J. G., and Ryu, K. H.: Landslide susceptibility mapping in Injae, Korea, using a decision tree, Eng Geol, 116(3), 274–283, 2010. https://doi.org/10.1016/j.enggeo.2010.09.009

74. Yesilnacar, E., and Topal, T.: Landslide susceptibility mapping : A comparison of logistic regression and neural networks methods in a medium scale study, Hendek region (Turkey), Eng Geol, 79(3), 251–266, 2005. https://doi.org/10.1016/j.enggeo.2005.02.002

75. Yilmaz I.: Comparison of landslide susceptibility mapping methodologies for Koyulhisar, Turkey: conditional probability, logistic regression, artificial neural networks, and support vector machine, Environ Earth Sci 61(4), 821-836, 2010. https://doi.org/10.1007/s12665-009-0394-9

76. Yu, F. C., Chen, T. C., Lin, M. L., Chen, C. Y., and Yu, W. H.: Landslides and rainfall characteristics analysis in Taipei City during the Typhoon Nari event, Nat. hazards, 37(1), 153–167, 2006. https://doi.org/10.1007/s11069-005-4661-0

77. Zhou, W., Tang, C., Van Asch, T. W., and Zhou, C.: Rainfall-triggering response patterns of post-seismic debris flows in the Wenchuan earthquake area, Nat. Hazards, 70(2), 1417–1435, 2014. https://doi.org/10.1007/s11069-013-0883-8
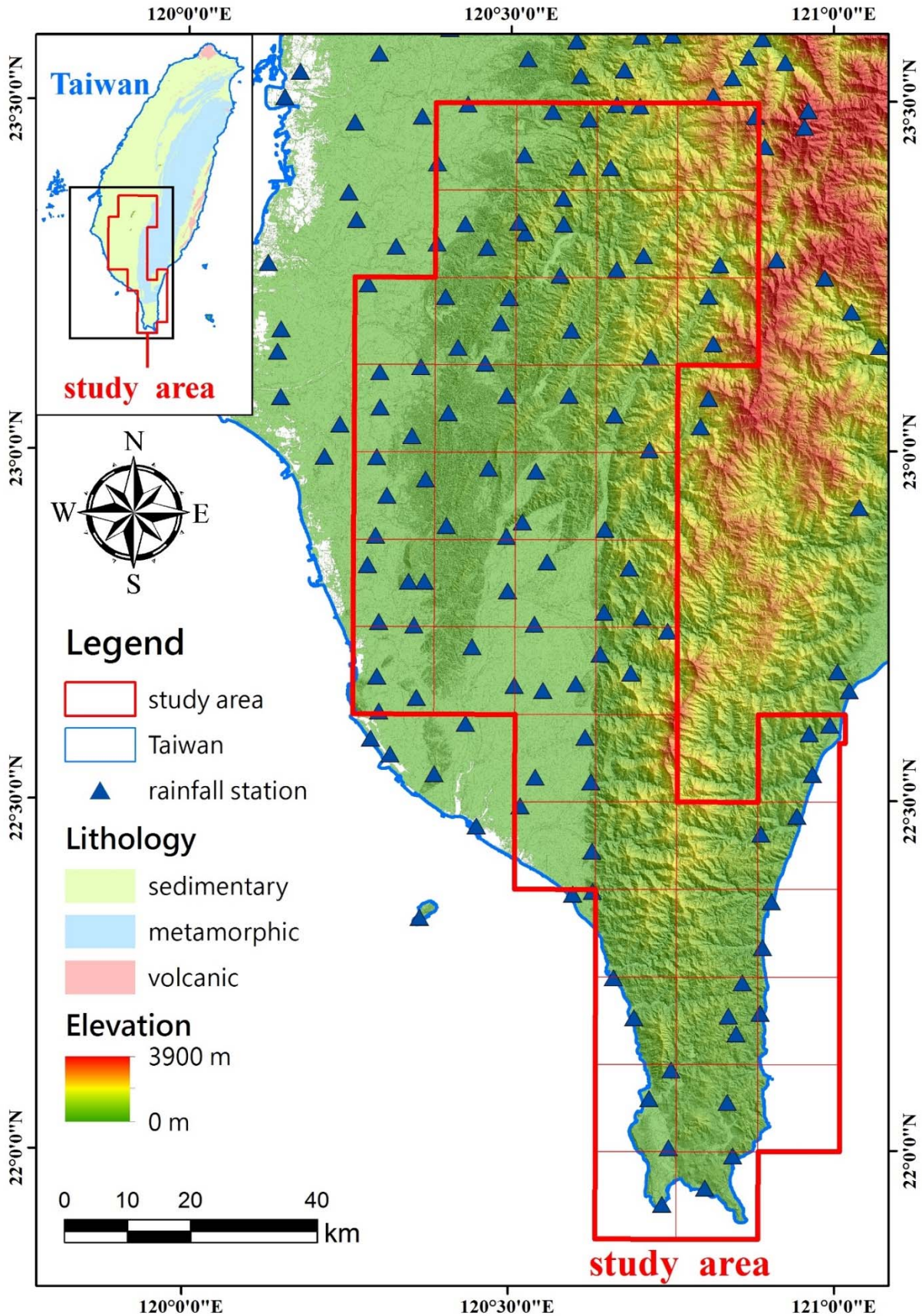
Figure 1: Geomorphological and geological settings of the study area. The elevation ranges from 3,243 meters in the eastern mountain area to sea level in the western plains area. Lithological units are mainly metamorphic rocks in the Central Range and sedimentary rocks in the Western Foothills. Rainfall data of 423 stations in Taiwan (96 of which are located in the study area) were collected for the interpolation and analysis of the triggering rainfall of landslides.
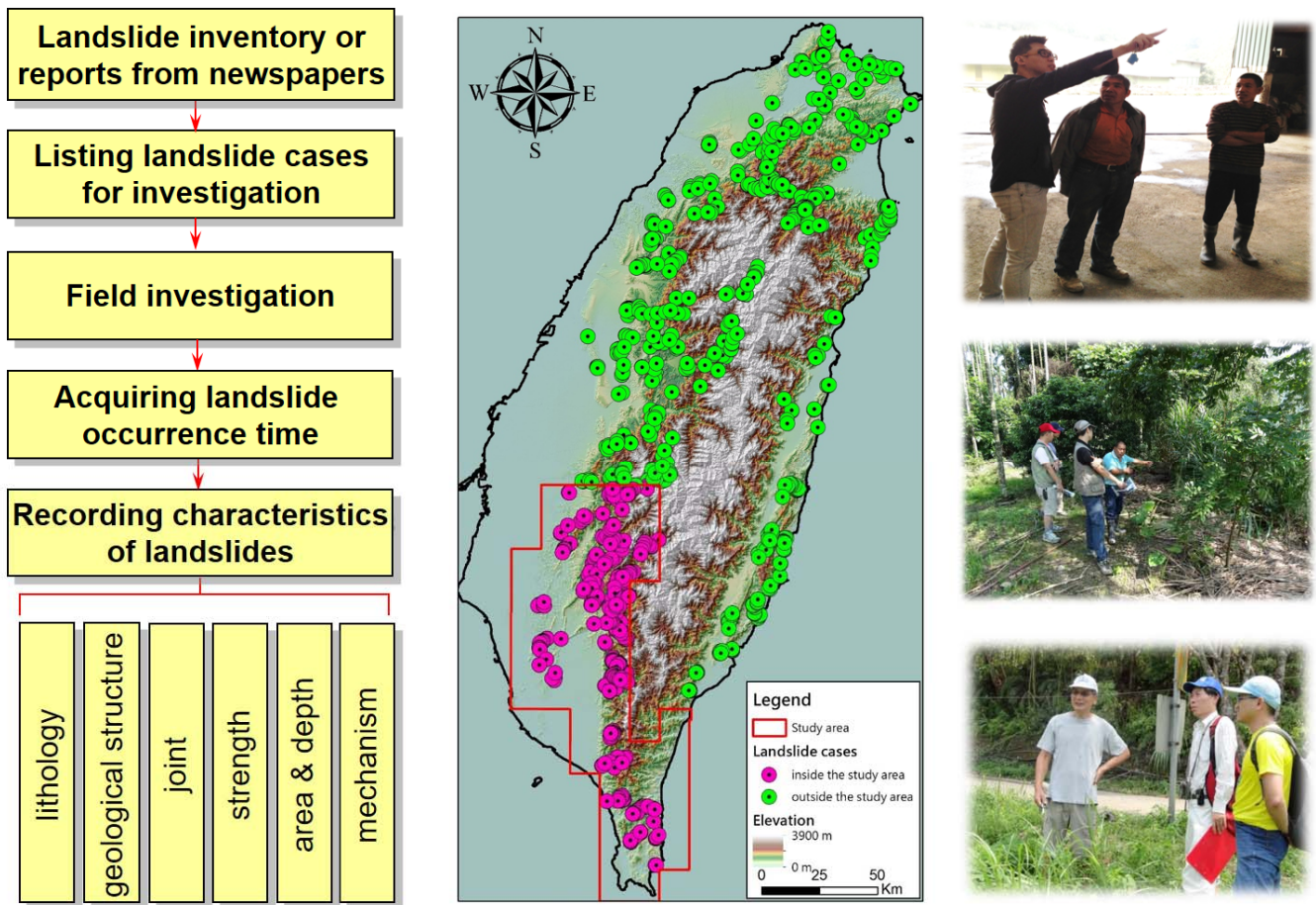
**Figure 2: Flowchart of landslide occurrence time gathering during field investigation (left), locations of landslide cases with the occurrence times used in this study (middle), and the pictures of interviewing residents (right). To improve the quality of this key information, landslide occurrence times were obtained from local residents, especially those whose relatives were injured or houses were damaged/destroyed by the landslides.**
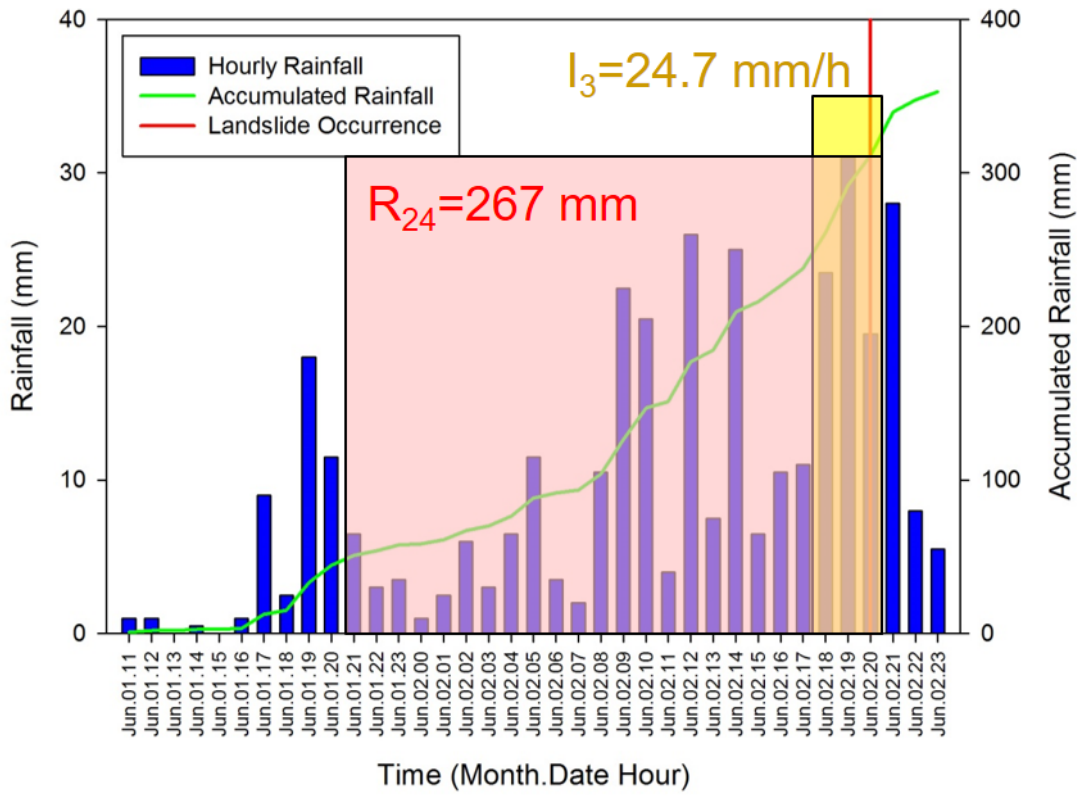
**Figure 3: 3-hour mean rainfall intensity ($I_3$) and 24-hour accumulated rainfall ($R_{24}$) were used as short-term and long-term rainfall indexes for the establishment of rainfall thresholds.**
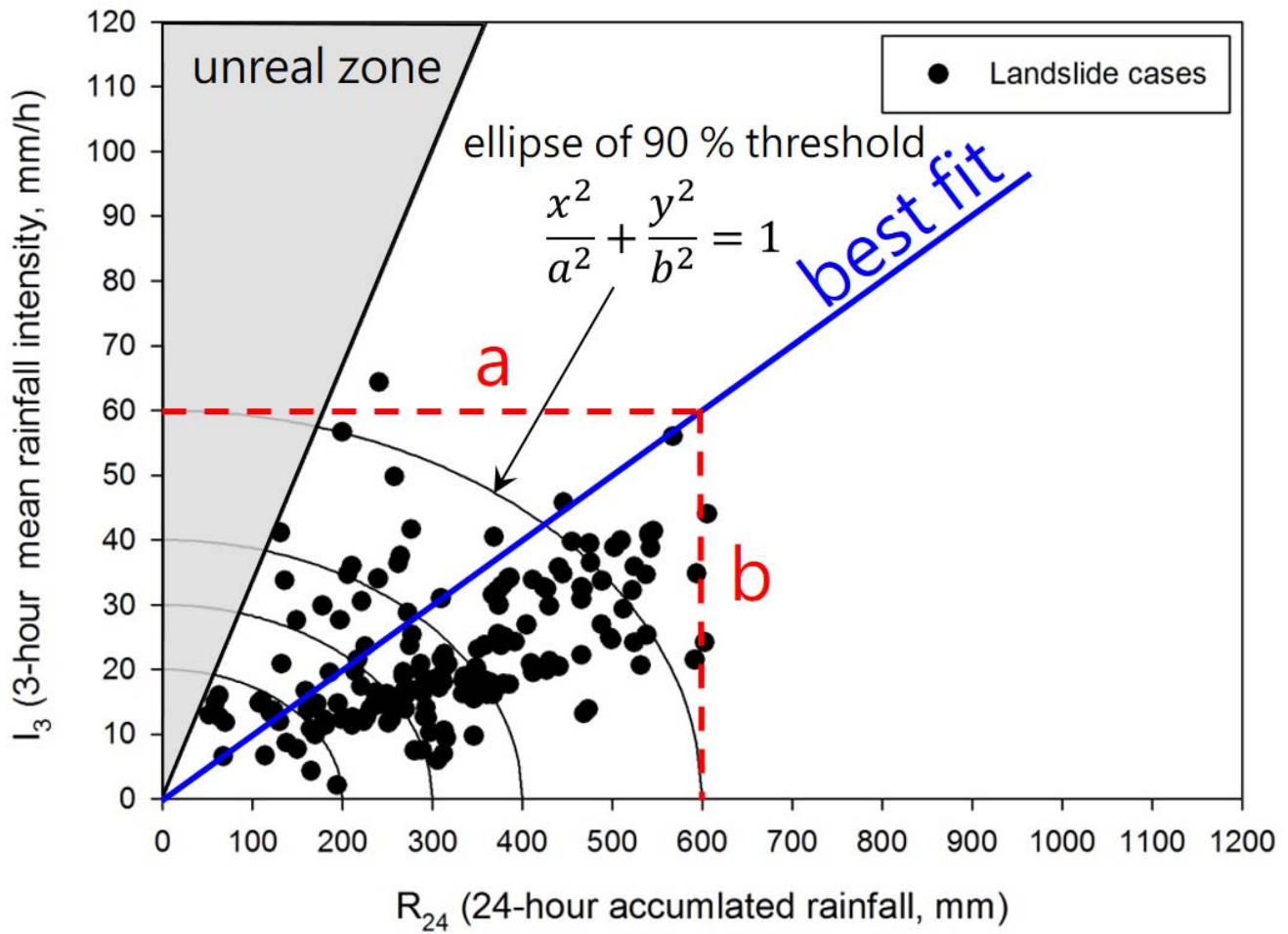
**Figure 4: Establishment of $I_3$–$R_{24}$ rainfall thresholds for shallow landslides. The best fit line was derived by least square method, and the ratio of a and b was used as the ratio of the semi-major axis and semi-minor axis in the ellipse threshold line.**

| | | Rainfall threshold (T) | | | |
|---|---|---|---|---|---|
| | | $T_{90\%}$ | $T_{60\%}$ | $T_{30\%}$ | $T_{15\%}$ |
| **Landslide susceptibility** | High susceptibility | Extreme danger level | Extreme danger level | High danger level | Medium danger level |
| | Moderate susceptibility | Extreme danger level | High danger level | Medium danger level | Low danger level |
| | Low susceptibility | High danger level | Medium danger level | Low danger level | Low danger level |

**Figure 5: Landslide early warning model and alert considering both landslide susceptibility and rainfall thresholds.**
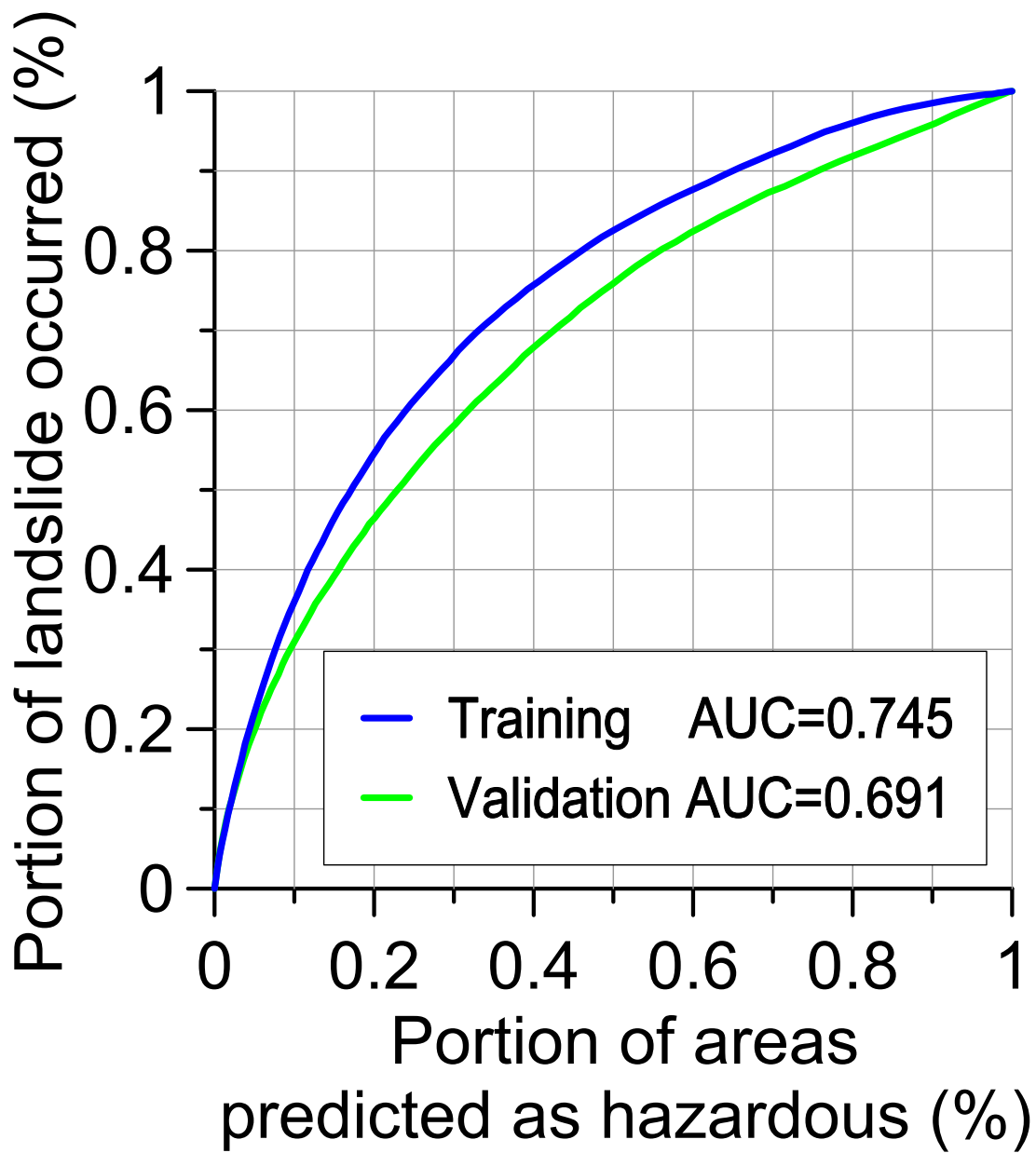
Figure 6: Area under the curve (AUC) of training and validation of landslide susceptibility analysis.

## (a) High susceptibility
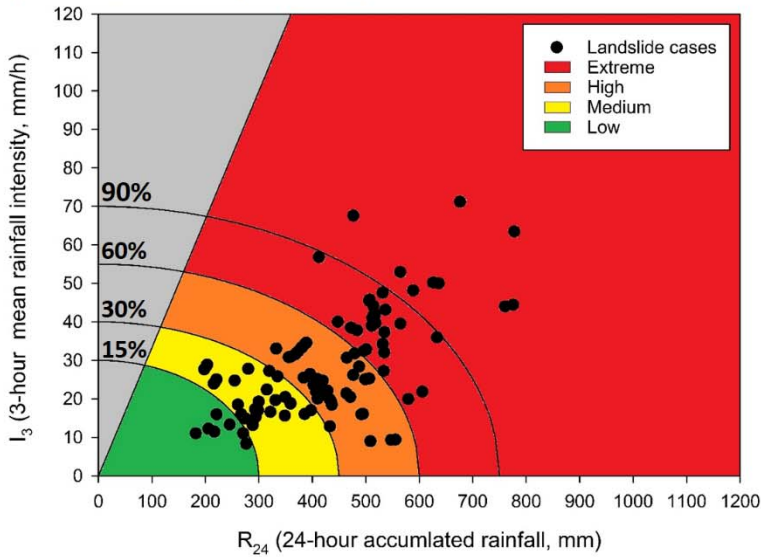
## (b) Moderate susceptibility
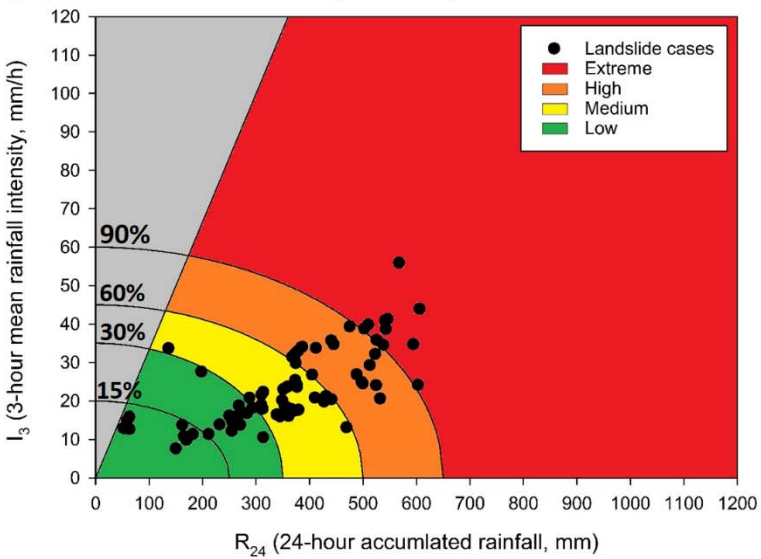
## (c) Low susceptibility
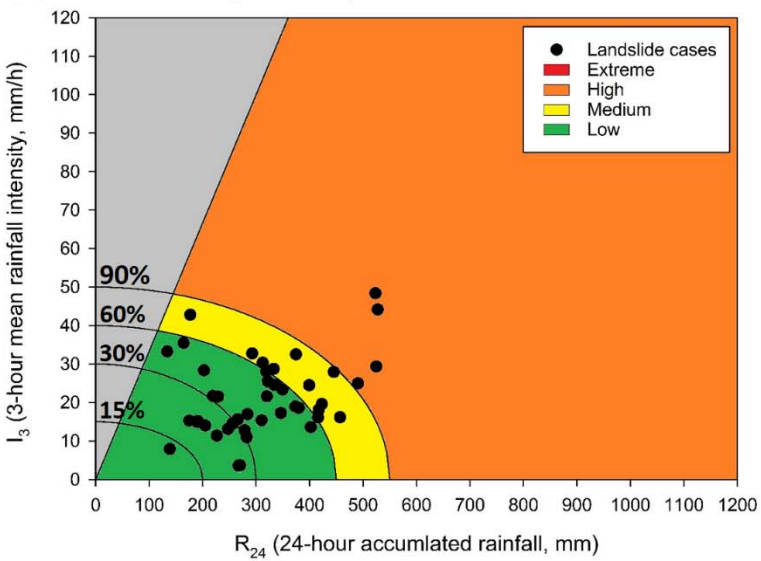
**Figure 7: $I_3$–$R_{24}$ rainfall thresholds and alert of (a) high–susceptibility slope units (b) moderate susceptibility slope units and (c) low–susceptibility slope units for southern Taiwan.**

| Landslide susceptibility | Rainfall threshold (T) | | | | | | | |
|---|---|---|---|---|---|---|---|---|
| | $T_{90\%}$ | | $T_{60\%}$ | | $T_{30\%}$ | | $T_{15\%}$ | |
| | $I_3$ | $R_{24}$ | $I_3$ | $R_{24}$ | $I_3$ | $R_{24}$ | $I_3$ | $R_{24}$ |
| High susceptibility | 70 (68) | 750 (745) | 55 (56) | 600 (610) | 40 (40) | 450 (438) | 30 (27) | 300 (291) |
| Moderate susceptibility | 60 (61) | 650 (657) | 45 (46) | 500 (498) | 35 (34) | 350 (368) | 20 (22) | 250 (236) |
| Low susceptibility | 50 (50) | 550 (539) | 40 (40) | 450 (430) | 30 (29) | 300 (316) | 15 (15) | 200 (167) |

**Figure 8: Rainfall thresholds for southern Taiwan. The values were calculated as 90%, 60%, 30%, and 15% of the original threshold respectively. After that, $I_3$ was rounded to the nearest 5 mm/h and $R_{24}$ was rounded to the nearest 50 mm for operational purpose (e.g., evacuation). The original values are shown in parentheses.**
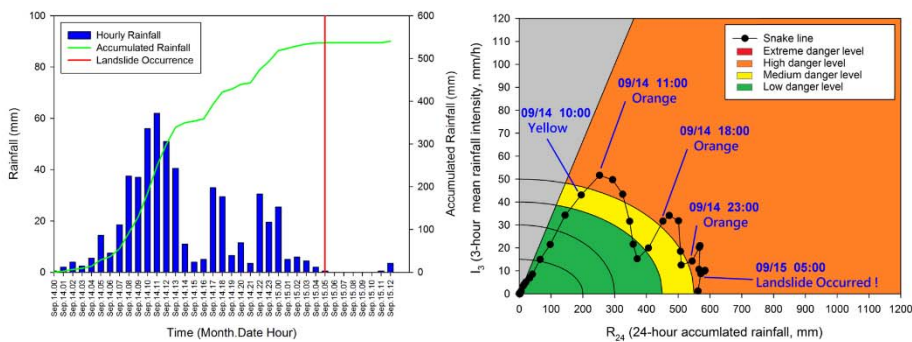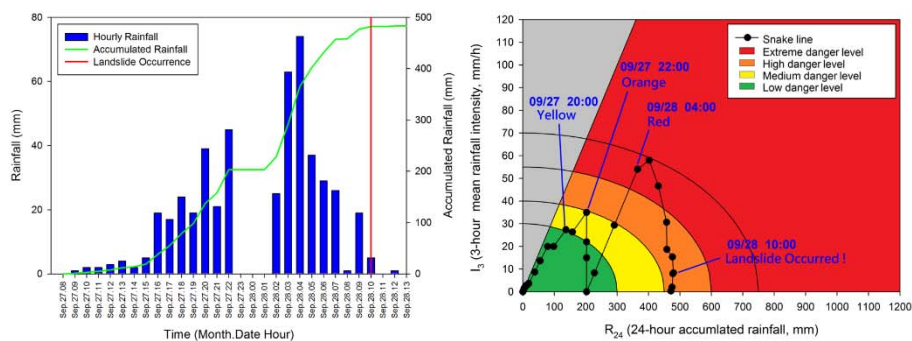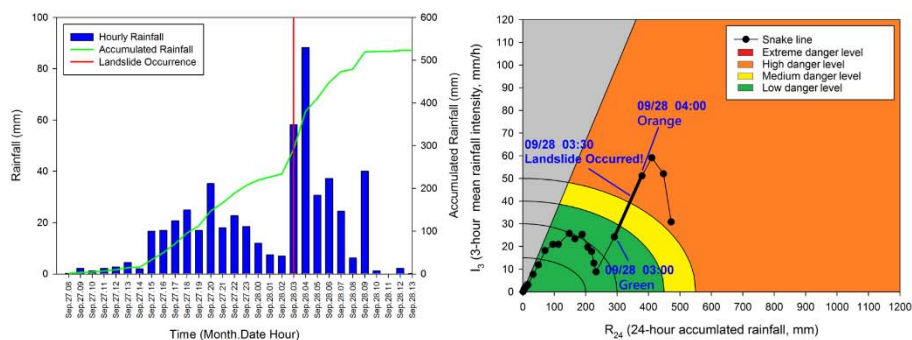
**Figure 9: Disastrous landslide cases in 2016, their rainfall histograms, and their snake lines in the I₃–R₂₄ diagram. The results showed that orange or red alerts could have been issued in advance for these disastrous landslides.**
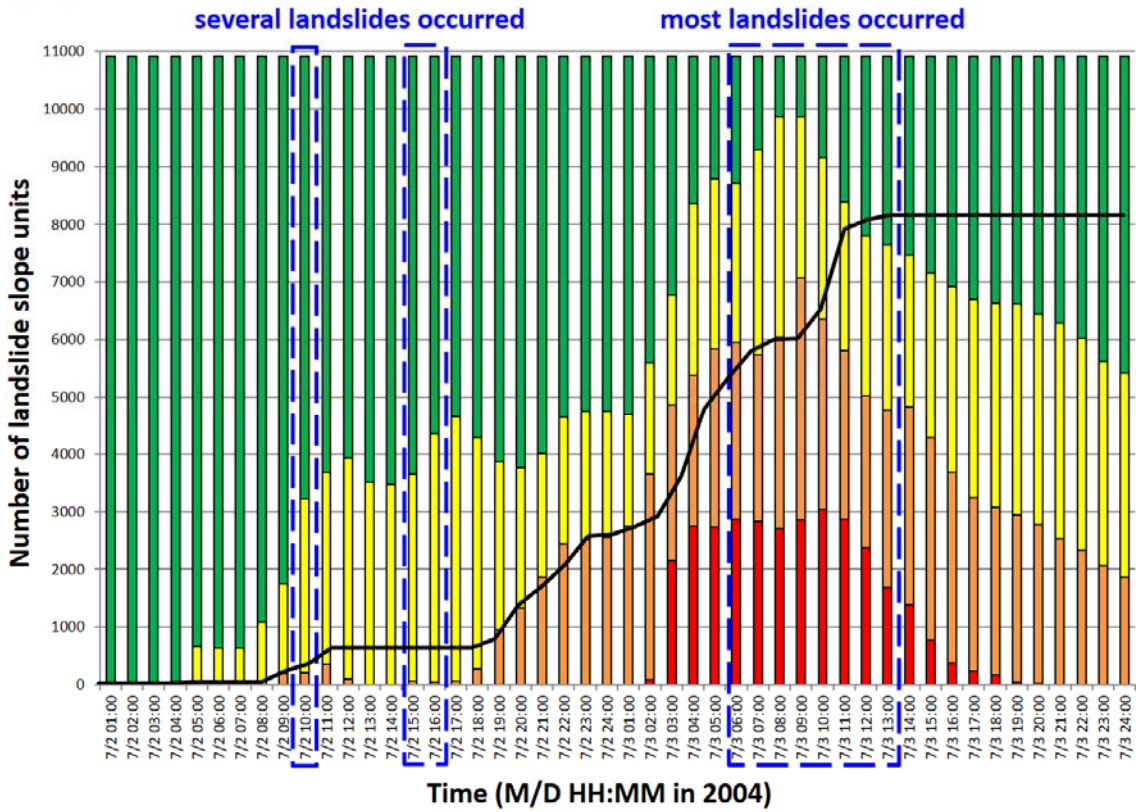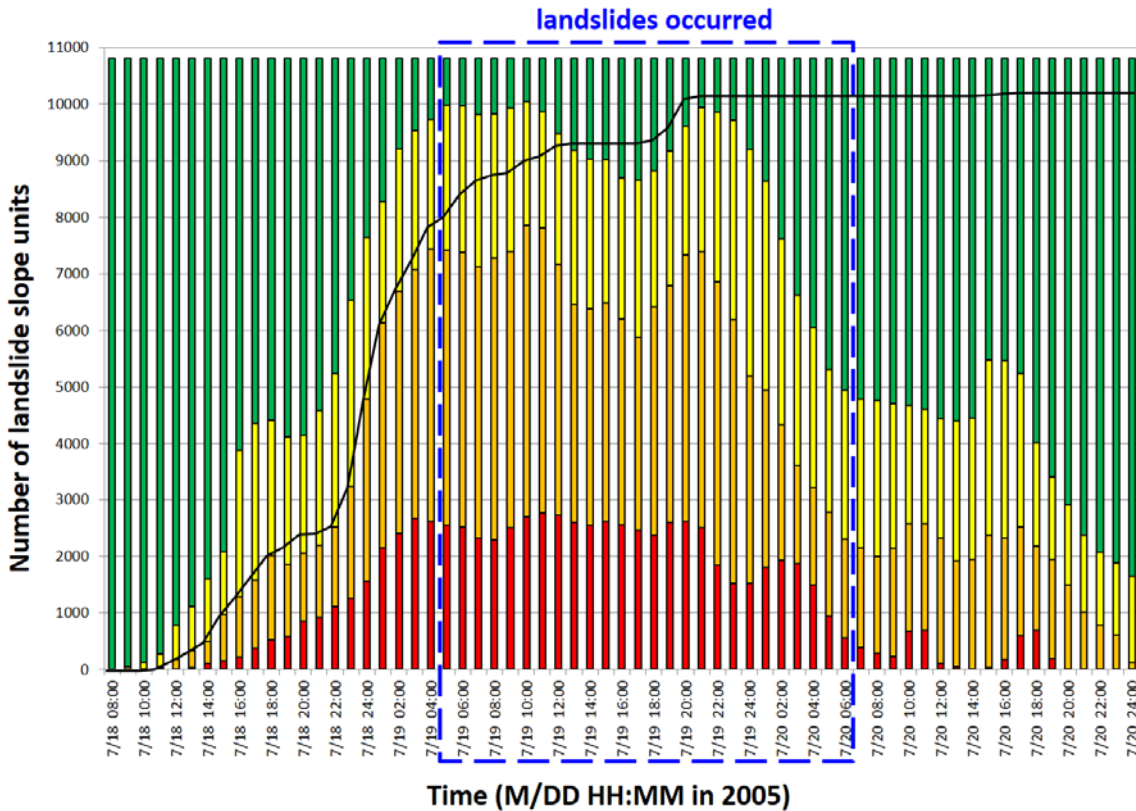
**Figure 10: Warning history of (a) Typhoon Mindulle and (b) Typhoon Haitang showing that the time at which our model issued alerts matched the landslide occurrence times reported by newspapers.**

**Table 1: List of landslide inventories generated in this study.**

| Year | Event |
|------|-------|
| 2004 | Before Typhoon Mindulle |
| 2004 | After Typhoon Mindulle |
| 2005 | After Typhoon Haitang |
| 2006 | After 0609 torrential rainfall |
| 2007 | After Typhoon Sepat |
| 2008 | After Typhoon Sinlaku |
| 2009 | After Typhoon Morakot |

**Table 2: Predisposing factors and their coefficient in logistic regression analysis.**

| Code | Factor item | coefficient |
|------|-------------|-------------|
| $L_{01}$ | RMSSC I | - |
| $L_{02}$ | RMSSC II | - |
| $L_{03}$ | RMSSC III | -0.874 |
| $L_{04}$ | RMSSC IV | -0.099 |
| $L_{05}$ | RMSSC V | 0.314 |
| $L_{06}$ | RMSSC VI | -0.384 |
| $L_{07}$ | RMSSC VII | - |
| $F_{01}$ | dip slope | 0.207 |
| $F_{02}$ | average slope | 0.265 |
| $F_{03}$ | variance of slope | 0.098 |
| $F_{04}$ | ratio of steep slope | 0.344 |
| $F_{05}$ | average curvature | 0.016 |
| $F_{06}$ | variance of curvature | 0.161 |
| $F_{07}$ | fold density | 0.013 |
| $F_{08}$ | average wetness | 0.061 |
| $F_{09}$ | 3-hour mean rainfall intensity ($I_3$) | -0.817 |
| $F_{10}$ | 24-hour accumulated rainfall ($R_{24}$) | 0.665 |
| C | Constant | 0.057 |

5  **Table 3: Type and the proportion of landslide occurrence times.**

| type of landslide occurrence time | amount (percentage) |
|-----------------------------------|---------------------|
| Type A: within the 3 hours following the highest rainfall intensity (landslide induced by high rainfall intensity) | 218 (23%) |
| Type B: within the 3 hours following the 2nd or 3rd highest rainfall intensity (landslide induced by high rainfall intensity) | 242 (26%) |
| Type C: near the end of the rainfall event (landslide induced by high accumulated rainfall) | 481 (51%) |
| Total | 941 (100%) |

**Table 4: Coefficient of variation of different accumulated rainfall indexes.**

| Accumulated rainfall Indexes | Coefficient of Variation |
|---|---|
| 6-hour accumulated rainfall ($R_6$) | 0.68 |
| 12-hour accumulated rainfall ($R_{12}$) | 0.47 |
| 24-hour accumulated rainfall ($R_{24}$) | 0.38 |
| 48-hour accumulated rainfall ($R_{48}$) | 0.41 |
| 72-hour accumulated rainfall ($R_{72}$) | 0.45 |

**Table 5: Contingency matrix for the validation of landslide early warning model. Shown are four outcomes: True Positive (TP), True Negative (TN), False Positive (FP) and False Negative (FN).**

| | | Observed events | |
|---|---|---|---|
| | | Yes | No |
| Forecasted events | Yes | True Positive (TP) | False Positive (FP) |
| | No | False Negative (FN) | True Negative (TN) |

**Table 6: Alerts and the corresponding danger levels, as well as suggested actions.**

| Alert | Danger level | Suggested action |
|---|---|---|
| Green | Low | - |
| Yellow | Medium | Notice announcements |
| Orange | High | Evacuation |
| Red | Extreme | Forced evacuation |

**Table 7: Disastrous landslide cases in 2016 and the results of validation. Warnings could have been issued for all landslide cases in advance or at the time of occurrence.**

| Landslide susceptibility | Lithology | Landslide area | Alert & issuing time | Occurrence of Landslide | Early (+) Late (-) |
|---|---|---|---|---|---|
| Shihwen landslide (Shihwen villiage, Chunri Township, Pingtung County) | | | | | |
| Low | Weathered sandstone | 61,500 m$^2$ | Orange, 11:00, 14-Sep, 2016 | 05:00, 15-Sep, 2016 | +18 hours |
| Zhongmin landslide (Zhongmin Rd., Yanchao District, Kaohsiung City) | | | | | |
| High | Mudstone interbedded with thin sandstone | 3,500 m$^2$ | Orange and red, 04:00, 28-Sep, 2016 | 10:00, 28-Sep, 2016 | + 6 hours |
| Houcuo landslide (Houcuo Ln., Qishan District, Kaohsiung City) | | | | | |
| Low | Conglomerate | 4,000 m$^2$ | Orange, 03:00 – 04:00, 28-Sep, 2016 | 03:30, 28-Sep, 2016 | 0 hour |

**Table 8: Validation of warnings issued for slope units and the hit rate during Typhoons Mindulle and Haitang.**

| Typhoon event (year) | Landslide occurrence time reported by newspapers | Number of landslide slope units (Number of high-, moderate-, low-susceptibility slope units) | Number of slope units for which orange alerts had been issued | Hit rate |
|---|---|---|---|---|
| Mindulle (2004) | Mainly 06:00 – 13:00, 3-Jul, 2004 | 10,911 (5,129; 2,750; 3,032) | 8,283 | 75.9% |
| Haitang (2005) | From 05:00, 19-Jul to 06:00, 20-Jul, 2005 | 10,804 (2,592; 2,355; 5,857) | 10,245 | 94.8% |

**Table 9: Validation of alerts issued for villages during Typhoons Mindulle and Haitang by using contingency matrix and skill scores.**

| | | Observed events | | | | |
|---|---|---|---|---|---|---|
| | | Typhoon Mindulle (in 2004) | | | Typhoon Haitang (in 2005) | |
| | | Yes | No | | Yes | No |
| Forecasted | Yes | 220 | 30 | Yes | 194 | 24 |
| events | No | 9 | 77 | No | 28 | 12 |
| POD | | 0.961 | | | 0.874 | |
| POFD | | 0.280 | | | 0.667 | |
| POFA | | 0.120 | | | 0.110 | |